BULLETIN OF THE POLISH ACADEMY OF SCIENCES
TECHNICAL SCIENCES, Vol. 66, No. 4, 2018
DOI: 10.24425/124260



# Fractional model of the electrochemical capacitor relaxation phenomenon

V. MARTYNYUK[1], M. ORTIGUEIRA[2], M. FEDULA[1*], and O. SAVENKO[1]

[1] Khmelnitsky National University, Instytutska, 11, 29016, Khmelnytskyi, Ukraine
[2] UNINOVA and Faculty of Sciences and Technology of Universidade Nova de Lisboa, Campus da FCT da UNL, Quinta da Torre, 2825-149 Caparica, Portugal

**Abstract.** The fractional model of the electrochemical capacitor (EC) relaxation phenomenon is presented herein. The EC relaxation phenomenon occurs when EC impedance measurements are performed after charge or discharge current interruption during potential relaxation. The EC fractional model is obtained based on the fractional order transfer function, obtained in turn by means of fitting the EC impedance data. The inverse Laplace transform is used to obtain the EC impulse response. Meanwhile, the EC charge and discharge simulations are performed using the EC impulse response.

**Key words:** electrochemical capacitor transfer function, impulse response, potential relaxation, electrochemical impedance spectroscopy.

## 1. Introduction

The current development of electronics and power systems requires designing new energy storage devices with greater densities of energy and power [1–3].

The electrochemical capacitors (ECs) [4], known also as double layer capacitors, supercapacitors or ultracapacitors, accumulate electric energy just like traditional electrolytic capacitors. At the same time, ECs have large capacitances (thousands of farads), very small active resistance (milliohms or hundreds of micro-ohms) and, in contrast with accumulator batteries, they can perform thousands of charge/discharge cycles [1, 4]. The most significant characteristics of ECs are high power delivery and long exploitation time. The power density of ECs is considerably higher in comparison with accumulator batteries [1–5]. The electrical characteristics of ECs are suitable for a variety of high current applications such as hybrid electric vehicles (EV) [1, 6], power electronics and telecommunications, where short, high-power pulses are required [2–4].

Also, at present time ECs are used in electronics for constructing electrical filters, oscillators and other devices, especially in the case of high requirements regarding phase characteristics in the frequency domain [7].

The main difference between ECs and conventional capacitors is the principle of energy storage. ECs use the electric double layer (EDL) for accumulation of electrical energy. They consist of two electrodes which are separated with a separator, as shown in Fig. 1. The electrodes are saturated with an electrolyte [4].

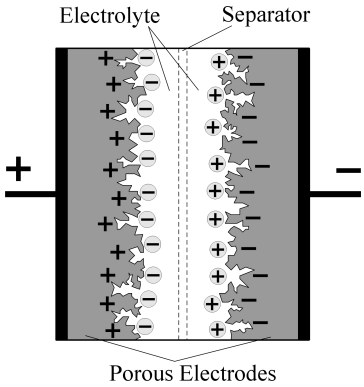


Fig. 1. Electrochemical capacitor structure

The value of energy stored by the EC depends on the area of its electrodes. Thus maximization of the EC electrodes' area is one of the most important problems in designing and manufacturing modern ECs. For this purpose, different materials and structures are used to increase the maximum energy and power density of the EC [3, 4]. Traditional materials used in EC electrodes include carbon aerogels, nanotubes and nanopowders [8]. Meanwhile, modern researches concentrate on development of new EC electrode materials, such as graphene [9] or biomaterials [10], and on more exact engineering of the electrode structure, resembling that of e.g. fractal capacitors [11].

The disadvantage of ECs is their low operational voltage, typically from 2.7V to 3.3V [4]. To overcome this disadvantage, ECs are connected in series and packed in modules [3]. Thus it is very important to seek out ECs with similar electrical parameters because if the electrical parameters of the serial connected ECs are different, then they are charged at different speeds [3, 4]. For example, EC number 3 that is shown in Fig. 2 has the lowest capacitance and the highest active resistance. Other ECs are not charged completely and

*e-mail: mailfm2000@gmail.com

Manuscript submitted 2017-11-15, revised 2018-01-08, initially accepted for publication 2018-01-10, published in August 2018.

the total module voltage is less than the working module voltage. In this case we continue to charge the module and the voltage of EC number 3 exceeds the critical value $V_{max}$. This leads to damage of EC number 3 and then to damage of the module.

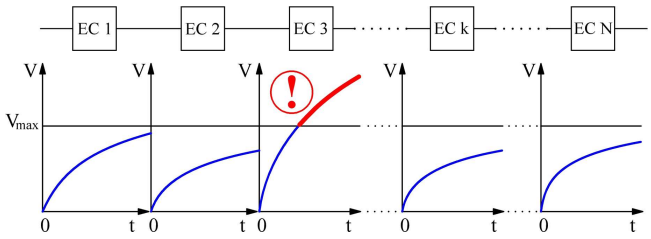


Fig. 2. Exceeding critical voltage values for EC number 3

To provide protection from exceeding the critical voltage values for all ECs in the module, it is necessary to measure the impedance of ECs and then sort out ECs for the module with similar electrical parameters.

Thus the correct and exact modeling of EC behavior is one of the most important goals for efficient application of ECs in modern electrical devices.

## 2. Present state of EC modeling techniques development

Analogously to EC electrodes having complicated structures with large areas [4, 8], the EC equivalent circuit does not match the simple models based on a single capacitor with series and parallel parasitic resistances [4, 5]. The single-capacitor EC models suffer from massive fitting errors and thus they are used in electrical engineering only for approximate estimation of EC characteristics [3].

The real equivalent circuit of the EC is a complex RC-network with distributed parameters [4, 12]. The more exact EC models are based on representations of the EC equivalent circuit in one of Cauer or Foster forms [12–15].

The other approach to EC modeling is based on the expression of an EC equivalent circuit as a long line with distributed parameters [13, 16, 17]. The pointed models with distributed parameters can provide good fitting accuracy but the disadvantage of such models lies in using hyperbolic functions in the expression of EC impedance. They make the time-domain model analysis more difficult, as per the limitations of Laplace transform [18].

In general, traditional EC models [4, 12–17] approximate the EC impedance spectrum with high accuracy but they have significant disadvantages:

- the elements of traditional EC equivalent circuits do not correspond to the parameters of EC materials such as carbon electrodes and electrolyte;
- the mathematical expressions for describing the EC impedance functions are complicated;
- for long-line based EC models, it is difficult to perform the inverse Laplace transform of the EC impedance function to find the expression of transient resistance and simulate the EC charge or discharge processes in the time domain.

Therefore modern approaches to EC modeling are based on application of fractional calculus [19, 20], which overcomes the above-described disadvantages of traditional models [4, 12–17]. In [13, 21] it was shown that EC electrodes with geometry characterized by self-similarity properties can be described by fractional-order models.

At present time, there are many different fractional order models of EC, such as the Warburg element [22], bounded Warburg element [23], Havriliak-Negami element [24], fractional impedance function with two fractional powers $\alpha$ and $\beta$ [25] and new multi-segment models [26–28].

In general, the pointed fractional order EC models can be described by means of the following equation [29, 30]:

$$Z(s) = R_0 + \frac{\sum\limits_{n=0}^{N} A_n \cdot s^{\alpha_n}}{\sum\limits_{m=0}^{M} B_m \cdot s^{\beta_m}}. \tag{1}$$

The fractional order models [26–30] provide much better capabilities for EC characteristics approximation than the integer order models [4, 12–17].

But in practice the fractional order EC models with vast numbers of numerator and denominator terms are not used in accordance with the complexity of evaluation of such models in the time domain, especially under the condition of parallel resistance presence that leads to using Mittag-Leffler functions [27, 31–33].

Thus, the most useful fractional order EC models consist of several fractional order segments and parasitic resistances [13, 26, 27]. Besides, for exact modeling of ECs in frequency and time domains, the accounting of transient processes' impacts is required [34–38]. Usually such transient processes are caused by relaxation [13].

In the time domain, the relaxation effects can be described by charge and discharge curves but the mathematical models of such processes are complicated, following the equivalent circuits of EC electrodes [4]. Therefore the modern techniques of EC modeling and parameter estimation include the analysis of non-stationary modes [37–39]. The investigation of EC characteristics in the non-stationary mode allows to determine the dependencies between relaxation processes and EC model parameters [13, 34, 37, 38].

Thus the EC modeling presented in this article is performed in stationary and non-stationary modes with using the three-segment fractional order impedance model.

## 3. Fractional order EC model selected

Most known fractional order EC models [13, 26–31] are based on the EC Nyquist plot that consists of two regions: the high frequency region with angle $\alpha \approx 45°$ and the low frequency region with angle $\gamma \approx 89°$. The experimental results obtained [26] for the EC impedance spectra show that a more accurate EC Nyquist plot has three main frequency ranges: the high frequency region with angle $\alpha \approx 45°$; the middle frequency range with angle $\beta \approx 75°$ and the low frequency range with angle $\gamma \approx 89°$, as shown in Fig. 5.

For the more accurate EC Nyquist plot, it is possible to write the EC transfer function that is described by Eq. (2) [26]:

$$H(s) = R + \frac{1}{s^a \cdot C_a} + \frac{1}{s^b \cdot C_b} + \frac{1}{s^{a+b} \cdot C_{a+b}}, \qquad (2)$$

where $R$ is active serial resistance, $C_a$, $C_b$ and $C_{a+b}$ are fractional capacitances and $a$ and $b$ are the orders of model segments.

The model (2) consists of three fractional order segments. The EC impulse response is defined with expression (3) by the inverse Laplace transform of the EC transfer function (2):

$$h(t) = R\delta(t) + \frac{t^{a-1}}{C_a \cdot \Gamma(a)} u(t) + \frac{t^{b-1}}{C_b \cdot \Gamma(b)} u(t) + \frac{t^{(a+b)-1}}{C_{a+b} \cdot \Gamma(a+b)} u(t), \qquad (3)$$

where $t$ stands for time, $\delta(t)$ is the Dirac delta function, $u(t)$ is the Heaviside unit step and $\Gamma(a)$ is the Euler Gamma function.

The selected model provides high fitting accuracy and allows to avoid complicated expressions of time-domain characteristics [26–30].

## 4. Investigation of EC model parameters in stationary mode

As a diagnostic technique for the electrical characterization of ECs under operating conditions, electrochemical impedance spectroscopy (EIS) [13, 14] is selected. According to EIS methods [13, 14], impedance measurements are performed under stationary mode conditions. In this case, the EC is at the equilibrium state.

In the stationary mode, impedance measurements are performed after stopping the transient processes, as shown in Fig. 3. The first stage (keys K1 and K2 in position 1) is the charge. The EC is charged with the constant current source. The second stage (keys K1 and K2 in position 2) is the potential relaxation. The current source is disconnected from the EC for a long time until the transient process finishes. The potential relaxation diagram is shown in Fig. 4.

The EC impedance spectra are shown in Fig. 5.

The EC voltage decreases from charge value $U_C$ to relaxation value $U_r$. Stage 3 (key K1 in position 2 and key K2 in position 3) is the impedance measurement. It is performed in the frequency range from $f_{\min} = 1$ mHz to $f_{\max} = 1$ kHz. The impedance spectrum obtained is shown in Fig. 5 (a) as a Nyquist plot.

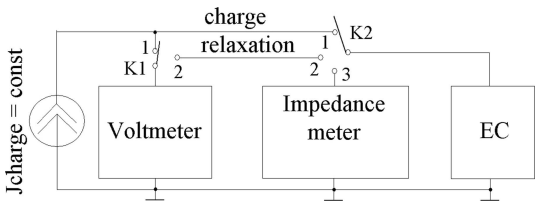


Fig. 3. Block diagram for EC parameters measurement in stationary mode

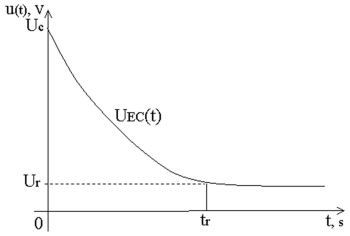


Fig. 4. Diagram of EC potential relaxation

a)

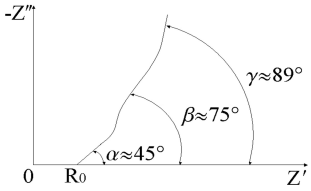


b)

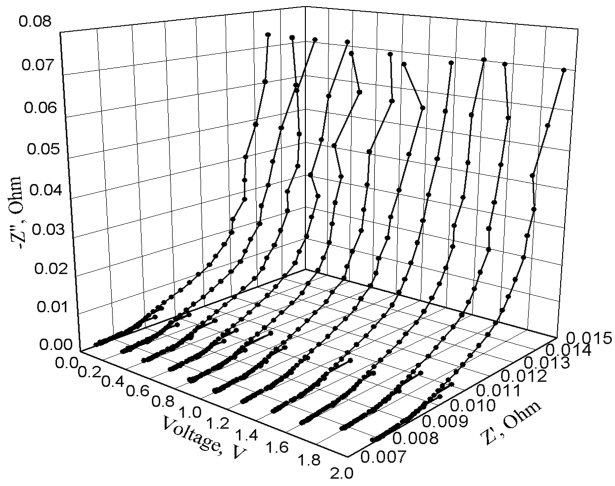


Fig. 5. EC impedance spectra: (a) schematic diagram of EC impedance spectrum at one charge voltage; (b) EC impedance spectra for voltage range from 0 V to 2 V

As shown in Fig. 5a, the impedance spectrum has three slopes with the following angles: $\alpha \approx 45°$ at the high frequency range; $\beta \approx 75°$ at the middle frequency range; and $\gamma \approx 89°$ at the low frequency range. The impedance measurements are performed for the EC working voltage range from $U_{\min} = 0$ V to $U_{\max} = 2$ V. The experimental impedance spectra are shown in Fig. 5 for the EC model HE0120C-0027A with nominal capacitance 120 F and rated voltage 2.7 V. It has been manufactured by Ness Capacitor Co., Ltd (South Korea).

## 5. Fractional EC model for stationary mode

The EC direct current test was conducted with constant current source $J = 1$ A = const. EC voltage was measured at the charging process. So, we have to find the EC unit-step response that is defined with equation (4) by means of integration of the EC impulse response (3):

$$h^1(t) = R + \frac{t^a}{C_a \cdot \Gamma(1+a)} + \frac{t^b}{C_b \cdot \Gamma(1+b)} + \frac{t^{a+b}}{C_{a+b} \cdot \Gamma(1+a+b)}. \qquad (4)$$

EC voltage can be found with multiplication of the EC unit-step response (4) by constant current $J = 1$ A = const, and defined by means of the following equation (5):

$$v(t) = v_0(t) + \left[R + \frac{t^a}{C_a \cdot \Gamma(1+a)} + \frac{t^b}{C_b \cdot \Gamma(1+b)} + \frac{t^{a+b}}{C_{a+b} \cdot \Gamma(1+a+b)}\right] \cdot J, \tag{5}$$

where $\nu_0(t) = 0.36$ V is the initial EC voltage. To find parameters $R$, $C_a$, $C_b$, $C_{a+b}$, $a$ and $b$, we performed the optimization procedure with the goal function $f(x)$ that is defined as the squared sum of the approximation error values for every sample in the frequency and time domains:

$$f(x) = p1 \cdot \sum_{k=1}^{N} \left(\mathrm{Re}(H\exp_k) - \mathrm{Re}(H(s_k, x))\right)^2 + p2 \cdot \sum_{k=1}^{N} \left(\mathrm{Im}(H\exp_k) - \mathrm{Im}(H(s_k, x))\right)^2 + p3 \cdot \sum_{m=1}^{M} \left(V\exp_m - V(t_m, x)\right)^2, \tag{6}$$

where $p_1$, $p_2$ and $p_3$ are weighted coefficients, $x$ is the optimization parameters vector, $H\exp_k$ is the $k$-th sample of the experimental EC transfer function and $H(s_k, x)$ is the $k$-th sample of the approximating EC transfer function. The approximation results are shown in Fig. 6.

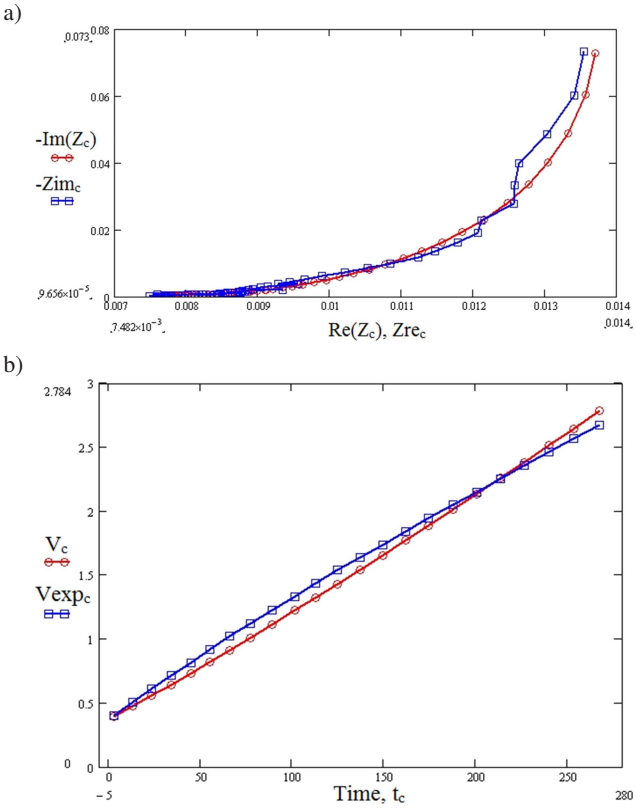


Fig. 6. EC approximation results: a) experimental EC impedance spectrum (blue line) and fitting curve (red line); b) experimental EC charge curve (blue line) and fitting curve (red line) in the time domain

After performing the optimization procedure, we obtained more parameters: $R = 7.39$ mOhm, $C_a = 130.21$ F/sec$^{1-a}$, $C_b = 308.64$ F/sec$^{1-b}$, $C_{a+b} = 296.74$ F/sec$^{1-(a+b)}$, $a = 0.2848$ and $b = 0.866$. The results thus obtained allow to perform the simulation of EC behavior with good accuracy in frequency and time domains, as shown in Fig. 6.

## 6. Investigating EC model parameters in nonstationary mode

The non-stationary mode of the electrochemical capacitor electrical parameters measurement is obtained by impedance spectroscopy operation during the relaxation process, with introducing the correction which corresponds to this process in digital processing of measurement results. A block diagram of EC parameters measurement is presented in Fig. 7.

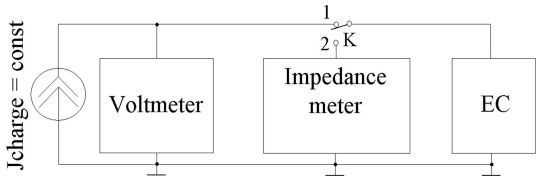


Fig. 7. Block diagram of EC parameters measurement in nonstationary mode

For the EC parameters control in the non-stationary mode, the measurement voltage is applied to the EC right away after EC charging or discharging. Total EC voltage is a sum of EC relaxation voltage and measurement voltage as shown in Fig. 8.

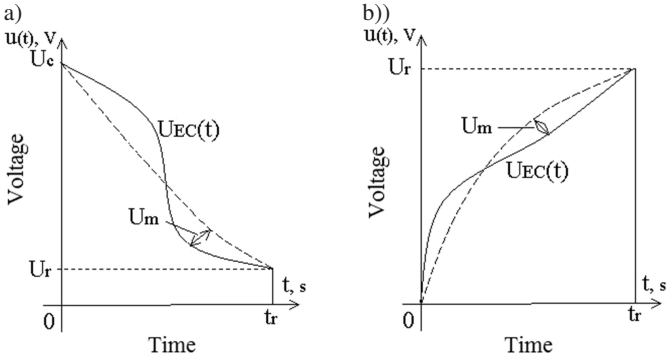


Fig. 8. EC voltage in the nonstationary control mode: a) total EC voltage after charging; b) total EC voltage after discharging

Total EC voltages after charging and discharging are described with expressions (7) and (8), respectively.

$$u_{EC}(t) = U_m \cos\omega_0 t + U_C e^{-\frac{t}{\tau_r}} + U_r, \tag{7}$$

$$u_{EC}(t) = U_m \cos\omega_0 t + U_r - U_r e^{-\frac{t}{\tau_r}}, \tag{8}$$

where $\tau_r$ is the EC time constant.

The impedance measurements are performed in the frequency range from $f_{\min} = 1$ mHz to $f_{\max} = 1$ kHz and the maximum charge (discharge) current values $I_{\max} = 1.8$ A. The impedance spectra obtained after EC charge and discharge

are presented in Fig. 9 which shows that EC impedance spectra in the non-stationary mode have a bend at ultralow frequencies. Moreover, this bend is more or less intensive and it also has the left or right direction. The shape of bend depends on the previous state of EC. If EC was charged before impedance measurement and there was no relaxation time between charging mode and impedance measurement, then the bend has a left direction as shown in Fig. 9a. The slope of bend depends on a value of the charge current and it can be significant for the high charge current values.

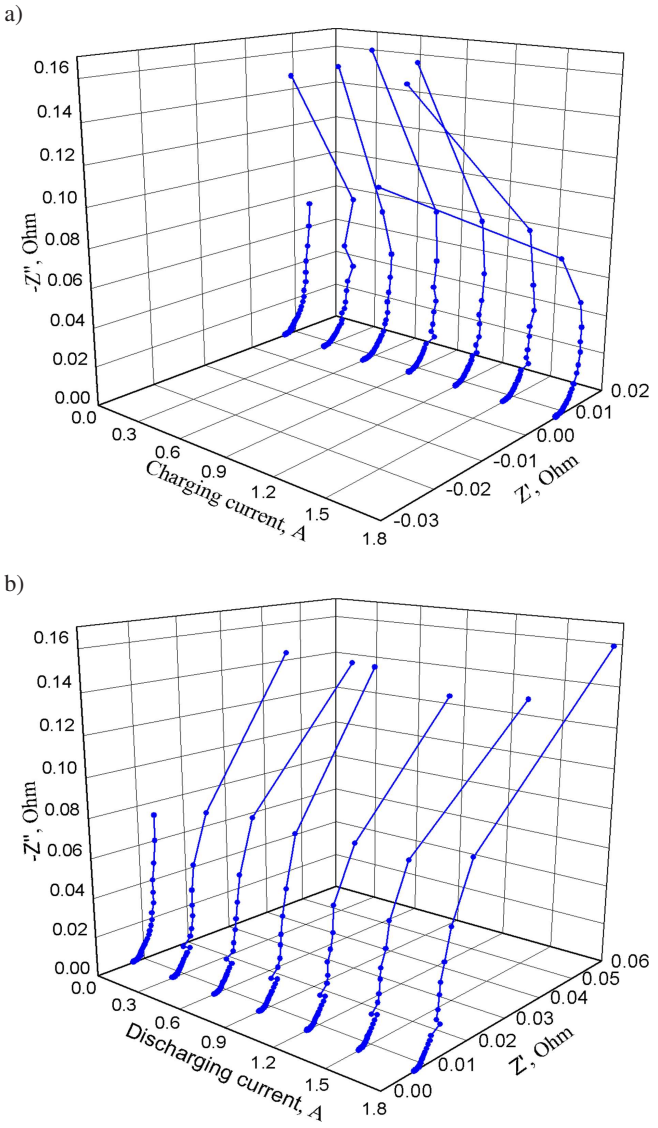


Fig. 9. Example EC impedance spectra in the nonstationary mode: a) EC impedance spectra after EC charging; b) EC impedance spectra after EC discharging

Here, we can see very interesting phenomenon when the real part $Z'$ of the EC complex impedance has negative values as shown in Fig. 9a. We called this phenomenon "EC relaxation phenomenon". We also can see that the negative values of the real part $Z'$ of the EC complex impedance depend on the values of charge current and they also depend on rated capacitance of EC.

On the other hand, if EC was discharged before impedance measurement and there was no relaxation time between discharging mode and impedance measurement, then the bend has a right direction as shown in Fig. 9b. In this case the slope of a band also depends on a value of the discharging current and the rated capacitance of EC that is like a previous case. However, there were no negative values of the real part $Z'$ of the EC impedance.

The origin of the EC relaxation phenomenon is explained by the relaxation process, which takes place inside EC following a fast charging/discharging process. Let us suppose that the EC is charged with electrical current $J = \text{const}$ up to voltage $U_C$, as shown in Fig. 10.

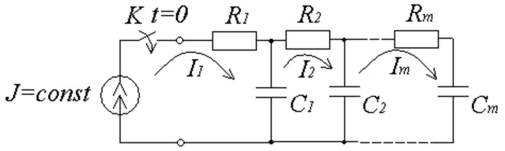


Fig. 10. Charging process of equivalent circuit EC

During the charging process, the current $J = \text{const}$ of the current source is divided into several currents: $I_1, I_2, \ldots, I_m$. These currents charge the following capacitances: $C_1, C_2, \ldots, C_m$ through resistors $R_1, R_2, \ldots, R_m$ and the current values are proportional to the values of resistors $R_1, R_2, \ldots, R_m$. Every branch is characterized by its time constant $\tau_i = R_i C_i$ and the charging times of every capacitance $C_1, C_2, \ldots, C_m$ to the voltage value of $U_C$ are also proportional to the time constant $\tau_i = R_i C_i$. The branch capacitance with minimum time constant $\tau_{\min}$ is charged to EC voltage $U_C$ first and then the charging process is terminated. On the other hand, all other capacitances have large time constants and they are not charged to EC voltage $U_C$.

When current source $J = \text{const}$ is disconnected from the EC, EC voltage falls down from the value of $U_C$ to the relaxation voltage of $U_r$ due to the redistribution of electrical charge between all capacitances of the EC equivalent circuit. During the discharging process, the current source $J = \text{const}$ discharges all capacitances $C_1, C_2, \ldots, C_m$ through resistors $R_1, R_2, \ldots, R_m$, as shown in Fig. 11. The capacitance to be discharged first has a minimum value and minimum discharging time constant. After that EC discharge is terminated. When current source $J = \text{const}$ is disconnected from the EC, EC voltage rises up from 0V to $U_r$ value due to the redistribution of an electrical charge of all capacitances of the EC equivalent circuit.

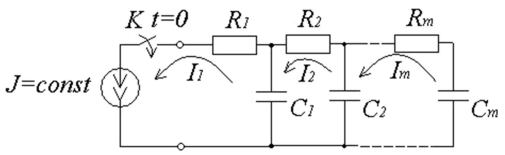


Fig. 11. Discharging process of equivalent circuit EC

A general outline of the EC impedance spectra in the stationary and non-stationary modes are shown in Fig. 12.

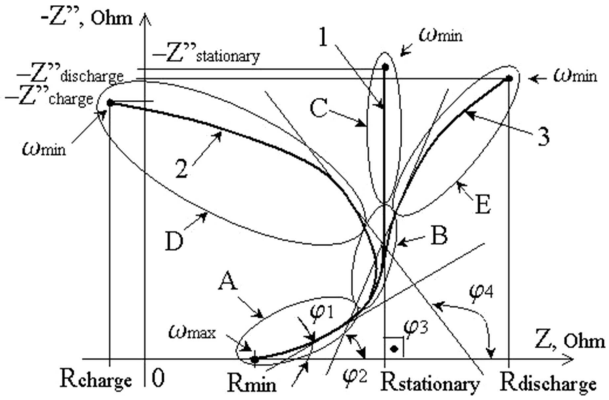


Fig. 12. EC impedance spectra in stationary and nonstationary modes

The EC impedance spectrum consists of three regions. If EC parameters control is performed in the stationary mode, the EC impedance spectrum trends to vertical line 1 that corresponds to region C, as shown in Fig. 12.

Region A corresponds to the high frequencies and the EC has a minimum value of active resistance $R_{\min}$ at maximum frequency $\omega_{\max}$. The tangent to the curve at the high frequency region A has angle $\varphi_1 < 90°$. The high frequency region A is common for the stationary and non-stationary modes because the time of the EC relaxation process is longer than the period of the high frequencies.

The next region, marked B, corresponds to the middle frequencies. At the middle frequency region B, the EC impedance spectra begin to disperse into three directions. In the stationary mode, the EC impedance spectrum trends to vertical line 1 that corresponds to the low frequency region C in the stationary mode. The tangent to the curve at the low frequency region C in the stationary mode has angle $\varphi_3 = 90°$. The maximum value of the EC active resistance is equal to $R_{\text{stationary}}$ at minimum frequency $\omega_{\min}$.

In the non-stationary mode, the EC impedance spectra disperse into two directions: left and right. The left direction corresponds to the low frequency region D when the EC parameters control is performed after EC charging. The tangent to the curve at the low frequency region D has angle $\varphi_4 > 90°$ in the non-stationary mode after charging. In this case the maximum value of the EC active resistance is equal to $R_{\text{charge}}$ at minimum frequency $\omega_{\min}$. The right direction corresponds to the low frequency region E when the EC parameters control is performed after EC discharging. In this case the tangent to the curve at the low frequency region E has angle $\varphi_2 < 90°$, similarly to the high frequency region A. In the non-stationary mode after discharge the maximum value of the EC active resistance is equal to $R_{\text{discharge}}$ at minimum frequency $\omega_{\min}$.

According to Fig. 12, the EC transfer function in the non-stationary mode is described with the following equation (9):

$$H(s) = R + \frac{1}{s^{\alpha} \cdot C_h} + \frac{1}{s^{\beta} \cdot C_m} + \frac{1}{s^{\gamma} \cdot C_l}, \qquad (9)$$

where $R$ stands for active serial resistance, $C_h$, $C_m$ and $C_l$ are fractional capacitances at the high, middle and low frequencies, respectively, and $\alpha$, $\beta$ and $\gamma$ are the orders at the high, middle and low frequencies, respectively. Taking transfer function (9) into account, the EC equivalent circuit for the non-stationary mode is shown in Fig. 13.

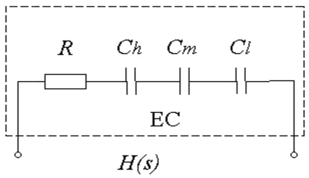


Fig. 13. EC equivalent circuit in the nonstationary mode

By using the EC transfer function in the non-stationary mode (9), the optimization procedure was performed for the impedance spectra obtained after EC charging and discharging (Fig. 3). Figure 14 shows the approximation results and the model orders after EC charging. The approximation results and the model orders after EC discharging are shown in Fig. 15.

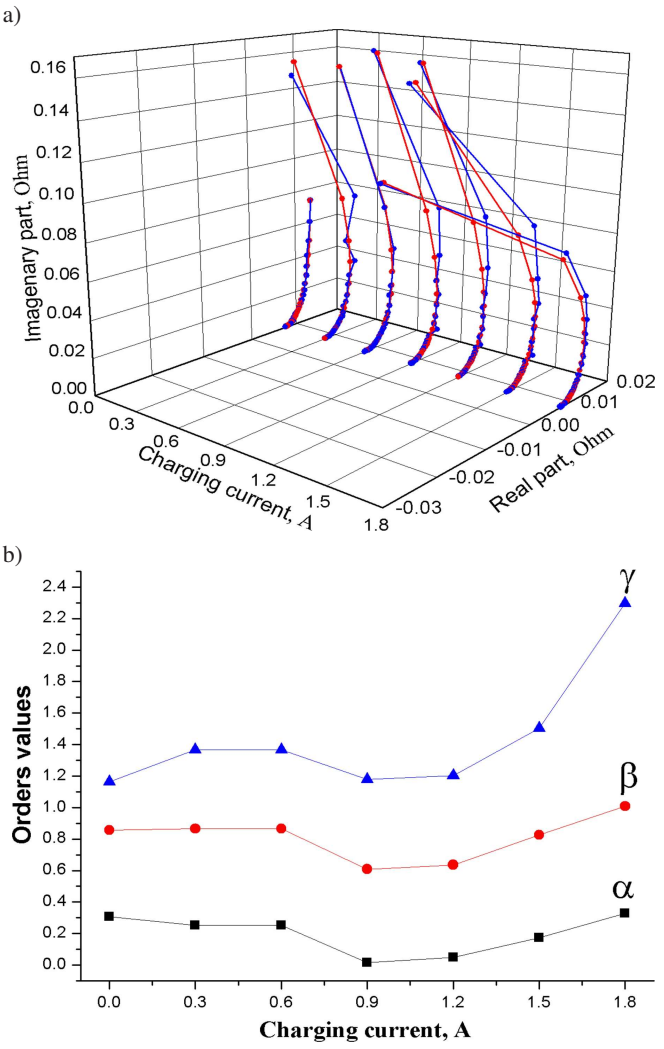


Fig. 14. EC impedance spectra and the model orders: a) EC impedance spectra and their approximation in the nonstationary mode after EC charging; b) the model orders vs. charging current

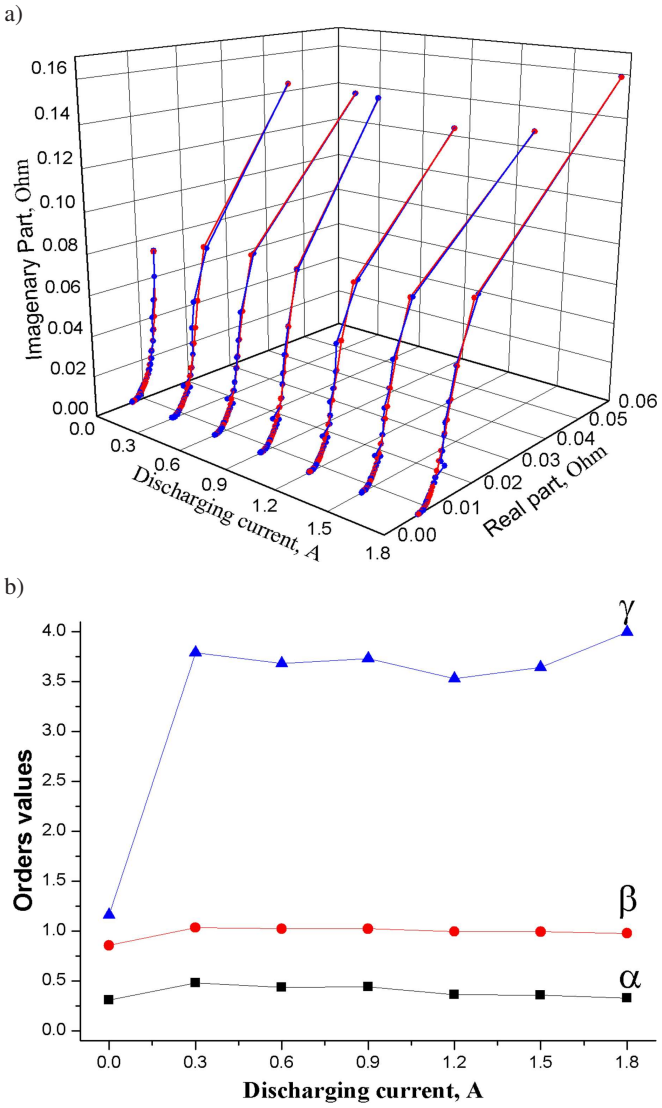


Fig. 15. EC impedance spectra and the model orders: a) EC impedance spectra and their approximation in the nonstationary mode after EC discharging; b) the model orders vs. discharging current

## 7. Conclusions

The results obtained by measuring electrical parameters of the EC with large nominal capacity depend considerably on the initial measurement conditions. Due to the fact that the equivalent circuit of the EC porous electrode is complex and equivalent to the long line [13, 16, 17], it is necessary while performing measurements to take into account the peculiarities of charge and discharge processes which took place before the measurement.

The figures displayed herein show that the value of the measured EC impedance depends greatly on the value of the current it was charged with, voltage and the form of transient processes.

In further research, it will be interesting to investigate the dependence (correlation) between transient processes when charging the EC to the initial voltage at which the measurement takes place and the differences between measurement results. This will further allow to introduce corrections that take account of transient processes in setting the EC impedance measurement mode.

Dependence figures (Fig. 14b and Fig. 15b) show wide prospects for the search of optimum EC running modes in order to obtain maximum equivalent capacity at transient processes and to store more energy.

Besides, as for the EC parameters measurement process, the non-stationary mode is more convenient because of its speed. The disadvantage of the EC stationary mode parameters control is the long time required after EC charge or discharge when the transient process in the EC is already finished. This time is defined with relaxation time $t_r$, as shown in Fig. 4, and it depends on the capacitance and active resistance of the EC. For an EC with nominal capacitance, i.e. hundreds or thousands farads, relaxation time $t_r$ is about 20 or 30 minutes. To overcome this disadvantage, it is necessary to perform the EC parameters control in the non-stationary mode, as shown in Fig. 7.

## REFERENCES

[1] V.S. Bagotsky, A.M. Skundin, and Yu.M. Volfkovich, *Electrochemical Power Sources. Batteries, Fuel Cells, and Supercapacitors*, The Electrochemical Society Series, Wiley, 2015.

[2] N. Kularatna, *Energy Storage Devices for Electronic Systems. Rechargeable Batteries and Supercapacitors*, Elsevier, 2015.

[3] M.-C. Pera, D. Hissel, H. Gualous, and Ch. Turpin, *Electrochemical Components*, John Wiley & Sons, Aug 2, 2013 – Technology & Engineering – 336 pages.

[4] B.E. Conway, *Electrochemical supercapacitors: Scientific Principles and Technological Application*, Plenum, New York, NY, 1999.

[5] S. Westerlung and L. Ekstam, "Capacitor Theory", *IEEE Transactions on Dielectrics and Electrical Insulation* 1(5), 826–839 (1994).

[6] B.E. Conway and W.G. Pell, "Double-layer and pseudocapacitance types of electrochemical capacitors and their applications to the development of hybrid devices", *Journal of solid State Electrochemical*, 7, 637–644 (2003).

[7] G. Tsirimokou, C. Psychalinos, and A. Elwakil, *Design of CMOS Analog Integrated Fractional-Order Circuits: Applications in Medicine and Biology*, Springer, Apr 12, 2017 – Technology & Engineering – 114 pages.

[8] K.I. Ozoemena and S. Chen, *Nanomaterials in Advanced Batteries and Supercapacitors*, Springer, 2016.

[9] Q. Ke and J. Wang, "Graphene-based materials for supercapacitor electrodes a review", *J. Mater.* 2, 37–54 (2016).

[10] X. Wang, D. Kong, Y. Zhang, B. Wang, X. Li, T. Qiu, Q. Song, J. Ning, Y. Song, and L. Zhi, "All-biomaterial supercapacitor derived from bacterial cellulose", *Nanoscale* 8(17), 9146 (2016).

[11] M. Ogorzalek, *Fractal Structures for Electronics Applications*, IEEE Circuits and Systems Society Workshop, 2007.

[12] S. Fletcher, V.J. Black, and I. Kirkpatrick, "A universal equivalent circuit for carbon-based supercapacitors", *Journal of Solid State Electrochemistry* 18(5), 1377–1387 (2014).

[13] E. Barsoukov and J.R. Macdonald, *Impedance Spectroscopy. Theory, Experiment, and Applications, 2-nd edition*, Wiley-Interscience, John Wiley & Sons, Inc, Hoboken, New Jersey, 2005. ISBN 0-471-64749-7.

[14] D. Vladikova, *The technique of the differential impedance analysis part I: Basics of the impedance spectroscopy*, In Proceedings of the International Workshop on Advanced Techniques for Energy Sources Investigation and Testing, pages 1–28, 2004.

[15] F.F. Kuo, *Network Analysis and Synthesis*, Wiley International, 5-th Edition, 2012.

[16] R. de Levie, "Electrochim", *Acta* 8, 751 (1963).

[17] M. Itagaki, Y. Hatada, I. Shitanda, K. Watanabe, "Complex impedance spectra of porous electrode with fractal structure", *Electrochimica Acta* 55, 6255–6262 (2010).

[18] A.D. Poularikas. *The Handbook of Formulas and Tables for Signal Processing*, CRC Press, 1999.

[19] M. Ortigueira, *Fractional calculus for scientists and engineers*, Springer, Berlin, 2011.

[20] M. Ortigueira and J. Machado, "Which Derivative?", *Fractal and Fractional* 1(1), 3 (2017).

[21] D. Ravaine and J.-L. Souquet, "Application du Trace des Diagrammes D'Impedance Complexe de la Determination de la Conductivité Electrique des Verres Silice-Oxyde Alcalin", *Compt. Rend. Acad. Sci. (Paris)* 277C, 489–492 (1973).

[22] G.W. Walter, "A review of impedance methods used for corrosion performance analysis of painted metals", *Corros. Sci.* 26(9), 681–703 (1986).

[23] V.S. Muralidharan, "Warburg impedance – basics revisited", *Anti-Corrosion Methods and Materials* 44(1), 26–29 (1997).

[24] R.R. Nigmatullin and S.I. Osokin, "Signal processing and recognition of true kinetic equations containing non-integer derivatives from raw dielectric data", *Signal Processing* 83(11), 2433–2453 (2003).

[25] J.J. Quintana, A. Ramos, and I. Nuez, *Identification of the fractional impedance of ultracapacitors*, In IFAC Workshop FDA. IFAC, 2006. ISBN 972-8688-42-3.

[26] V. Martynyuk and M. Ortigueira, "Fractional model of an electrochemical capacitor", *Signal Processing* 107, 355–360 (2015).

[27] T. Freeborn, B. Maundy, and A. Elwakil, *Fractional-order models of supercapacitors, batteries and fuel cells: a survey*, Materials for Renewable and Sustainable Energy, 2015.

[28] T.J. Freeborn, B. Maundy, and A.S. Elwakil, "Measurement of supercapacitor fractional-order model parameters from voltage-excited step response", *IEEE Journal on Emerging and Selected Topics in Circuits and Systems* 3(3), 416–424 (2013).

[29] C.A. Monje, Yang Quan Chen, B.M. Vinagre, Dingyü Xue, and V. Feliu, *Fractional-order Systems and Controls. Fundamentals and Applications*, Springer-Verlag, 2010.

[30] M. Lewandowski and M. Orzyłowski, "Fractional-order models: The case study of the supercapacitor capacitance measurement", *Bull. Pol. Ac.: Tech.* 65(4), 449–457 (2017).

[31] J.J. Quintana, A. Ramos, and I. Nuez, *Modeling of an EDLC with fractional transfer functions using Mittag-Leffler equations*, Math. Probl. Eng., Article ID 807034, 7 pp., 2013.

[32] V. De Santis, V. Martynyuk, A. Lampasi, M. Fedula, and M.D. Ortigueira, "Fractional-order circuit models of the human body impedance for compliance tests against contact currents", *International Journal of Electronics and Communications (AEÜ)* 78, 238–244 (2017).

[33] R. Gorenflo, A. Kilbas, F. Mainardi, and S. Rogosin, *Mittag-Leffler Functions, Related Topics and Applications: Theory and Applications*, Springer-Verlag Berlin Heidelberg, 2014.

[34] T. Kaczorek, "Relationship between the observability of standard and fractional linear systems", *Archives of Control Sciences* 27(LXIII)(3), 441–451 (2017).

[35] A. Jakubowska and J. Walczak, *Analysis of the Transient State in a Circuit with Supercapacitor*, Poznan University of Technology Academic Journals: Electrical Engineering, No 81, 2015.

[36] M. Fouda, A.S. Elwakil, A.G. Radwan, and A. Allagui, "Power and energy analysis of fractional-order electrical energy storage devices", *Energy* 111, 785–792 (2016).

[37] K. Darowicki, J. Orlikowski, and G. Lentka, "Instantaneous impedance spectra of a non-stationary model electrical system", *Journal of Electroanalytical Chemistry* 486(2), 106–110 (2000).

[38] K. Darowicki, K. Andrearczyk, P. Slepski, A. Sierczynska, G. Lota, K. Fic, and K. Lota, "Determination of pseudocapacitance changes of nickel oxide NiO electrode with the use of dynamic electrochemical impedance spectroscopy", *International Journal of Electrochemical Science* 9, 1702–1714 (2014).

[39] V. Gafiychuk and B. Datsko, "Mathematical modeling of different types of instabilities in time fractional reaction-diffusion systems", *Computers & Mathematics with Applications* 59(3), 1101–1107 (2010).